The EMBO Journal Vol. 20 No. 22 pp. 6213–6225, 2001

Structure of a fast kinesin: implications for ATPase mechanism and interactions with microtubules

Y.-H.Song[1], A.Marx, J.Müller, G.Woehlke[2], M.Schliwa[2], A.Krebs[3], A.Hoenger[3] and E.Mandelkow[1]

Max-Planck Unit for Structural Molecular Biology, D-22607 Hamburg, [2]Department of Cell Biology, Ludwig-Maximilians-University, D-80336 München and [3]EMBL, D-69117 Heidelberg, Germany

[1]Corresponding authors
e-mail: mand@mpasmb.desy.de or song@crystal.desy.de

We determined the crystal structure of the motor domain of the fast fungal kinesin from *Neurospora crassa* (NcKin). The structure has several unique features. (i) Loop 11 in the switch 2 region is ordered and enables one to describe the complete nucleotide-binding pocket, including three inter-switch salt bridges between switch 1 and 2. (ii) Loop 9 in the switch 1 region bends outwards, making the nucleotide-binding pocket very wide. The displacement in switch 1 resembles that of the G-protein ras complexed with its guanosine nucleotide exchange factor. (iii) Loop 5 in the entrance to the nucleotide-binding pocket is remarkably long and interacts with the ribose of ATP. (iv) The linker and neck region is not well defined, indicating that it is mobile. (v) Image reconstructions of ice-embedded microtubules decorated with NcKin show that it interacts with several tubulin subunits, including a central β-tubulin monomer and the two flanking α-tubulin monomers within the microtubule protofilament. Comparison of NcKin with other kinesins, myosin and G-proteins suggests that the rate-limiting step of ADP release is accelerated in the fungal kinesin and accounts for the unusually high velocity and ATPase activity.

Keywords: kinesin/microtubules/motor protein/*Neurospora crassa*

Introduction

Kinesin motor proteins accomplish various intracellular microtubule-based transport processes (reviewed in Goldstein and Philp, 1999; Woehlke and Schliwa, 2000). Conventional kinesin from animals consists of two heavy and two light chains, while kinesin from the fungus *Neurospora crassa* lacks the light chains. The heavy chain of conventional kinesin is organized into three domains: the N-terminal motor domain, the central stalk and the C-terminal light chain-binding domain. It is often associated with membranous organelles and responsible for their transport within the cell. Deletion of kinesin in *N.crassa* causes retarded hyphal growth and loss of the 'Spitzenkörper', an organelle linked to cell morphogenesis (Seiler *et al*., 1997).

The head domain of kinesin can be subdivided into a core motor domain of ~325 residues, responsible for the ATPase activity and microtubule (MT) binding, and a 'linker' region (residues ~325–340) connecting to the 'neck' (residues ~340–370), the beginning of the coiled-coil stalk. A number of kinesin structures have been solved so far, including forward and reverse motors: human kinesin (HsKin; Kull *et al*., 1996), Ncd monomer and dimer (Sablin *et al*., 1996, 1998), rat kinesin monomer and dimer (RnKin; Kozielski *et al*., 1997; Sack *et al*., 1997; Muller *et al*., 1999), Kar3 (Gulick *et al*., 1998), Kif1A (Kikkawa *et al*., 2001), Eg5 (Turner *et al*., 2001) and Kar3 mutants (Yun *et al*., 2001). These analyses have shown that the core nucleotide-binding domain is related to that of myosins and G-proteins (Rayment, 1996; Kull *et al*., 1998). Structures of G-proteins and myosins complexed with different nucleotides and nucleotide analogues (Coleman and Sprang, 1999; Gulick *et al*., 2000; Holmes and Geeves, 2000) have revealed that all these proteins might share a similar mechanism of nucleotide hydrolysis (Vale and Milligan, 2000). The γ-phosphate-sensing regions of the G- and motor proteins are formed by three elements: the P-loop, switch 1 (Sw1) and switch 2 (Sw2). During nucleotide hydrolysis, the proteins undergo a conformational change within the Sw1 and Sw2 regions. The γ-phosphate forms a hydrogen bond with the amide group of a conserved glycine (G60 in Ras, G457 in myosin II; Hilgenfeld, 1995; Scheidig *et al*., 1995; Furch *et al*., 1999; Gulick *et al*., 2000). The corresponding residues in kinesins are G238 in *N.crassa* kinesin (NcKin) or G235 in RnKin. In myosin, the chain at this glycine undergoes a peptide flip in the ADP state so that the amide is turned away from the γ-phosphate-sensing region (Smith and Rayment, 1996). This small conformational change triggers a cascade of structural alterations. They propagate from the P-loop to the Sw1 and Sw2 regions until they end in a distant region of the enzyme, which can then induce the dramatic movement of domains comparable with that seen in EF-Tu or in the swing of the lever arm in myosin (Hilgenfeld, 1995; Houdusse *et al*., 2000).

A key question is how this small difference in the active site can be transmitted to a distant location of the motor and modulate the affinity to the protein partners, e.g. MTs in the case of kinesin, F-actin for myosin, and the cofactors guanosine nucleotide exchange factor (GEF) or GTPase-activating protein (GAP) for the G-proteins (Hilgenfeld, 1995; Scheffzek *et al*., 1998; Holmes and Geeves, 2000). The case of kinesin is even more complicated because it is a highly processive motor and can take many steps along an MT before it dissociates. This is only possible if the two motor domains can communicate with each other. They achieve this by alternating site catalysis, whereby a transition in one head triggers a transition in the other (Hackney, 1996; Ma and

Taylor, 1997; Gilbert *et al*., 1998). In order to understand the mechanism, it would be helpful to know the structure of different types of kinesin in different states of the ATPase cycle. Here we describe the structure of a fungal kinesin that moves ~5 times faster than kinesins from animal sources (Steinberg and Schliwa, 1996; Seiler *et al*., 1997; Crevel *et al*., 1999), we show how it interacts with MTs and we discuss the basis of this high performance in comparison with other kinesins, myosin and G-proteins.

Results

General features of the structure

The structure of the motor domain of kinesin from *N.crassa* was solved by molecular replacement, using RnKin as a template [Protein Data Bank (PDB) code 2kin; Sack *et al*., 1997]. The model contains all 355 residues of the motor domain with one MgADP and 128 water molecules (Table I; Figure 1A and B). The fold of the protein is similar to that of other kinesins, as expected from the sequence homology (55% identity between NcKin and RnKin). The central eight-stranded β-sheet is surrounded by six α-helices, three on either side (red in Figure 1A and B). Figure 1B represents a rear view of the motor domain as seen from the inside of the MT, with the green elements (β5–L8, L11, α4–L12–α5) facing a β-tubulin subunit. The small lobe of NcKin (strands β1a, β1b and β1c) differs from that of RnKin by an insertion of four amino acids between β1b and β1c. There is also a large displacement in the MT-interacting region around β5a, β5b and the connecting loops (L8a and L8b) (Figure 1C and D). Helix α1 contains a bend which is common to all known kinesin structures. Helix α2 is interrupted through the 11 residue bulge loop L5, the longest interruption within α2 found in kinesin members. Interestingly, the greatest deviations between NcKin and RnKin are found in those regions that have been proposed to change conformation during the ATPase cycle, namely Sw1, Sw2 and the MT-binding surface. Helix α3 is 23 residues long, compared with 16 residues in RnKin, resulting in a 35 Å long helix. Helix α3a comprises only a half turn, much shorter than in other kinesin structures (Figure 1C and D). This alteration is remarkable as these residues belong to the Sw1 region and form part of the active site. L11, located close to both the nucleotide- and MT-binding regions, is ordered and thus visible, in contrast to other kinesin structures. Another region of interest is the transition from the core motor domain to the stalk (end of α6, residue ~325 for RnKin and ~329 for NcKin). This region was mostly disordered in the HsKin structure (Kull *et al*., 1996), but in RnKin showed an extended linker (β9 and β10, residues ~325–339) and the beginning of the α-helical neck (from ~339 onwards), which leads into the coiled-coil stalk domain and causes dimerization. In NcKin, the last 22 residues show weak density. The linker has an extended structure, similar to RnKin, but there is no evidence for an α-helical neck (Figure 1D, bottom right). This corresponds to a lower predicted helix-forming propensity in the initial segment of the neck region, compared with RnKin (Thormahlen *et al*., 1998). This region undergoes large structural transitions during the movement of kinesin and is probably intrinsically mobile (Rice *et al*., 1999).

Table I. Data collection and refinement statistics

Space group	$P2_12_12_1$
Unit cell parameters	a = 51.97 Å
	b = 72.73 Å
	c = 84.93 Å
Resolution range	30–2.3 Å
Reflections, observed/unique	138 093/14 829
Completeness, overall/last shell	99.8%/100%
R_{sym}[a], overall/last shell	9.9%/31.9%
Refinement statistics	
Resolution range	30–2.3 Å
R_{cryst} (%)[b]/R_{free} (%)[c]	21.9%/25.6%
Coordinate error, Luzzati/Sigmaa (Å)	0.32/0.21
R.m.s. deviations	
bond lengths (Å)	0.006
bond angles (°)	1.3
torsion angles (°)	23.3
improper torsion angles (°)	0.83

[a]$R_{sym} = \Sigma_{hkl}\Sigma_i|I_i - \langle I\rangle|/\Sigma_{hkl}\Sigma_i\langle I\rangle$ where I_i is the ith measurement of the reflection intensity I and is the weighted mean of all measurements of I.
[b]$R_{cryst} = \Sigma_{hkl}|F_{obs} - F_{calc}|/\Sigma F_{obs}$ where F_{obs} and F_{calc} are the observed and the calculated structure factors, and the summation is over 90% of reflections used for model refinement.
[c]R_{free}, as for R_{cryst} except summed only over the 10% of reflections not used for model refinement.

The unique structure of loop 11 and the switch 2 region of NcKin

A remarkable feature of NcKin is the ordered structure of L11 in the Sw2 region following strand β7. In part, it forms a secondary structure element resulting in the extension of β7 to β7a, which in turn follows a loop and continues along the novel helix α4a, extending the Sw2 helix α4 by 1.5 turns (Figure 2). This region is disordered in other kinesin structures, except possibly in the initial Ncd structure where an antiparallel sheet, β7a and β7b, was reported (Sablin *et al*., 1996). The sequence at the beginning of L11 (235-D**LAGSE**KVGKT-245 in NcKin) is highly conserved throughout all kinesins and contains the epitope of a widely used antibody (LAGSE motif, shown in bold; Sawin *et al*., 1992). The sequence also contains a GxxxxGKT motif (underlined above) which is typical of nucleotide-binding P-loops and prompted speculations about a second nucleotide-binding site (Steinberg and Schliwa, 1996). However, the structure of L11 shows that this region has no direct contact with the phosphate of the bound nucleotide, in contrast to the functional P-loop, residues 88–95; and other kinesins such as RnKin contain a serine instead of glycine at position 243, thus breaking the P-loop motif. Interestingly, there is a mutant of NcKin with a Gly243Ser exchange, as in the RnKin sequence (Figure 3). This mutant displays a 25% reduced growth rate of hyphae and a reduced MT gliding velocity (only 1.9 versus 2.6 μm/s; U.Henningsen and M.Schliwa, unpublished). It therefore appears that the nature of residue 243 is critical for kinesin velocity, and that structural transitions in L11 are important for the ATPase cycle.

The nucleotide-binding site

The nucleotide-binding pocket is formed by four elements, N1–N4 (Kull *et al*., 1996). They include highly conserved regions: (i) L1 (N4, motif 14-RxRP-17), which interacts

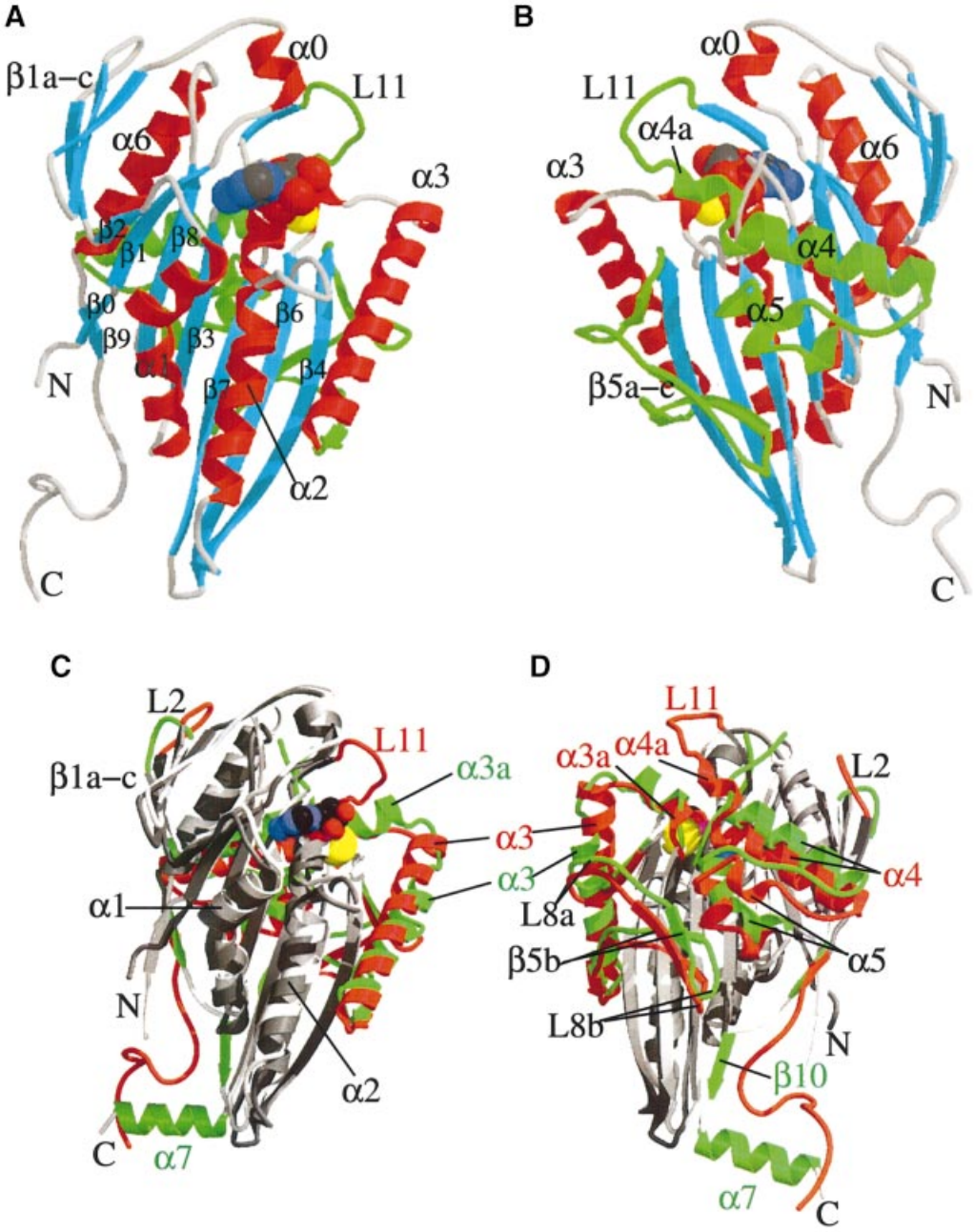

Fig. 1. (A and B) Ribbon diagram of the NcKin355 showing the overall fold. (**A**) Front view; (**B**) rear view, from the MT-binding surface. It is a globular structure with a central β-sheet of eight strands (β1–β8) and three α-helices on either side. α-helices (α0–α3, α6) are in red, and β-strands are in blue. The elements putatively involved in MT binding are coloured in green (α4–L12–α5, L11). ADP is shown as a space-filling model. (C and D) Comparison between the structures of NcKin and kinesin from rat brain. (**C**) Front view; (**D**) rear view. The structures of the NcKin and RnKin monomer (PDB code: 2kin) were superimposed by aligning the residues of the P-loops (NcKin 81–92, RnKin 97–92). Only regions with substantial variations in structure are shown in colour, NcKin in red and RnKin in green. L11 is ordered in the NcKin structure and elongates the Sw2 helix (α4) to α4a and the strand β7 to β7a. Helix α3 becomes longer (three turns more than in the RnKin structure) and α3a shorter. The interruption of the helix α2 is also longer. The linker region β9–β10 and following helical neck α7 of RnKin adopt a more disordered conformation in NcKin.

with the base; (ii) the phosphate-binding loop (N1 or P-loop, motif 88-GxxxxGKT-95); (iii) Sw1 (N2) including the region from α3a to β6 (motif 202-NxxSSR-207); and (iv) Sw2 (N3) including the region after β7 (motif 235-DLAGSE-240) and L11 (Figure 4A). Y96 at the end of the P-loop mediates a stacking interaction with the purine ring of the adenine base on one side, which corresponds to the histidine residue in RnKin (Muller *et al*., 1999). On the opposite side, the base makes a hydrophobic interaction with the ring of P16 and the hydrophobic portion of the side chain of R15. The adenine base is coordinated further through a water molecule (S123), which mediates a hydrogen bond between the base nitrogen N6 to the carbonyl oxygens of C59 and M57. The ribose oxygen O2′ binds a water molecule, which mediates a hydrogen bond to T101, a residue of the bulge loop L5 between α2a and α2b. This is of special interest because such a coordination of the ribose moiety has not been reported in any other

known kinesin structure. The coordinating T101 is an inserted residue in comparison with the sequence of RnKin and HsKin (Table II) and might play a role in the fast NcKin ATPase cycle. In the case of Ncd, a mutation of the conserved G446 to arginine in L5 causes complete loss of the function of the protein (Endow and Komma, 1997).

The bulge loop L5 of the plus motors is generally longer than that of the minus motors. Since L5 is close to the P-loop and is also part of the nucleotide 'entrance', the length of this loop might influence the ATPase cycle. The bridge oxygen between the α- and β-phosphate builds a hydrogen bond to the amide nitrogen of G93 at the end of the P-loop. The Mg^{2+} ion is coordinated octahedrally by six oxygen atoms also found in the nucleotide-binding pocket of RnKin (Muller *et al*., 1999). This includes a substrate oxygen atom on the β-phosphate, the side chain oxygen of S95 and four water molecules.

Access to nucleotide-binding pocket and switch 1 region

The terms 'open' and 'closed' applied to the pockets of the active site originate from the G-protein and myosin structures and refer to the movement of Sw1 and Sw2 relative to each other. The 'closed' conformation is usually found in the presence of ATP or GTP and their analogues (Mittal *et al*., 1996; Coleman and Sprang, 1999; Gulick *et al*., 2000). The distance between the conserved glycine at the beginning of the P-loop (G86 in RnKin) and the conserved glycine in the LAGSE motif of Sw2 (G235 in RnKin) has been taken as a measure for the openness of the nucleotide-binding pocket (Sack *et al*., 1999). In NcKin, this distance (G88–G238; 5.99 Å) is almost the same as in the structure of RnKin (5.87 Å) and Kar3 (5.82 Å). This means that the nucleotide-binding pocket of NcKin and the other kinesins can be considered as 'closed' even when the bound nucleotide is ADP, not ATP. Considering that the ATPase cycle contains several subreactions, the single criterion of the G88–G238 distance is likely to over-simplify the movements of Sw1 and Sw2. We therefore looked for other criteria to describe the accessibility of the nucleotide pocket in kinesin. The entrance of the nucleotide is at loops L1–L3–L5 and L9 (Figure 4B, green). The size of the pocket is determined critically by the position of L9, which belongs to the Sw1 region. In the case of Kar3, this loop is bent so far inwards that the active site becomes much smaller (Gulick *et al*., 1998). Therefore, the distance between the conserved glycine of the P-loop (G88) and the conserved asparagine of L9 in Sw1 (N202) would be an alternative measure of the openness of the pocket. In NcKin, the two residues (G88 and N202) are 22.7 Å apart, while for RnKin the corresponding distance (between G86 and N199) is 15.8 Å. Thus, this distance distinguishes between kinesin family members with different activities. Note that the minus motors (Ncd and Kar3) form a bulge loop between α3 and α3a (Figure 5B), whereas the plus motors do not (Figure 5A). Thus, besides the short distance between the

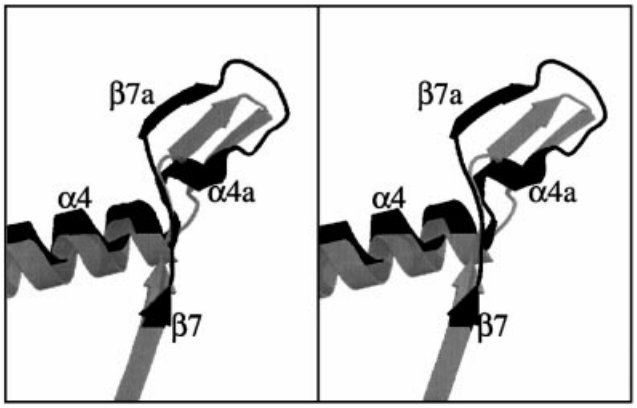

Fig. 2. Comparisons between the Sw2 structures of NcKin (black) and Ncd (grey) in ribbon representations. The orientation of the view is the same as in Figure 1. The switch 2 helix α4 and the strand β are somewhat extended into the L11 region.

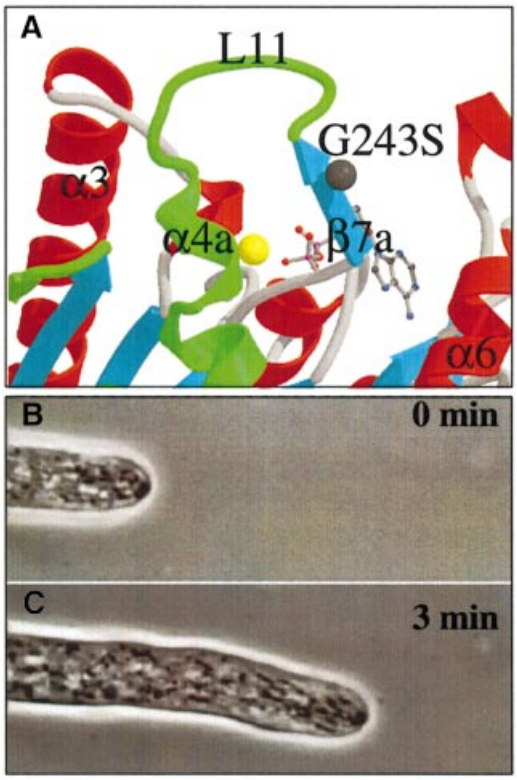

Fig. 3. Loop 11 and the growth rate of hyphae. (**A**) Conformation of L11 (residues 240–253), starting at strand β7a and ending at the short helix α4a, an extension of the switch 2 helix α4. Residue G243 is partly responsible for the high velocity of NcKin. (**B** and **C**) Growth of hyphae observed by phase-contrast microscopy. There is a time delay of 3 min between micrographs (B) and (C); the growth rate is 8.5 μm/min. Note the dark 'Spitzenkörper' at the tip.

Fig. 4. (**A**) Nucleotide-binding site and the coordination of ADP. Stereo diagram of the active site with bound ADP with its electron density, calculated as an omit map ($F_o - F_c$), and contoured at 1.5σ (see text). (B–D) The size of the nucleotide-binding pocket (stereo views). (**B**) Ribbon representation of the structure of NcKin. (**C**) Surface potential representation of the nucleotide-binding pocket of NcKin. (**D**) Kar3. The surface potentials are contoured according to the surface charge, with red denoting acidic and blue basic regions. The active site of NcKin is the most spacious among the known structures of kinesin motors. Figures were prepared using the programs SPOCK (Christopher, 1998) and Raster3d (Merrit, 1994); see Supplementary data.

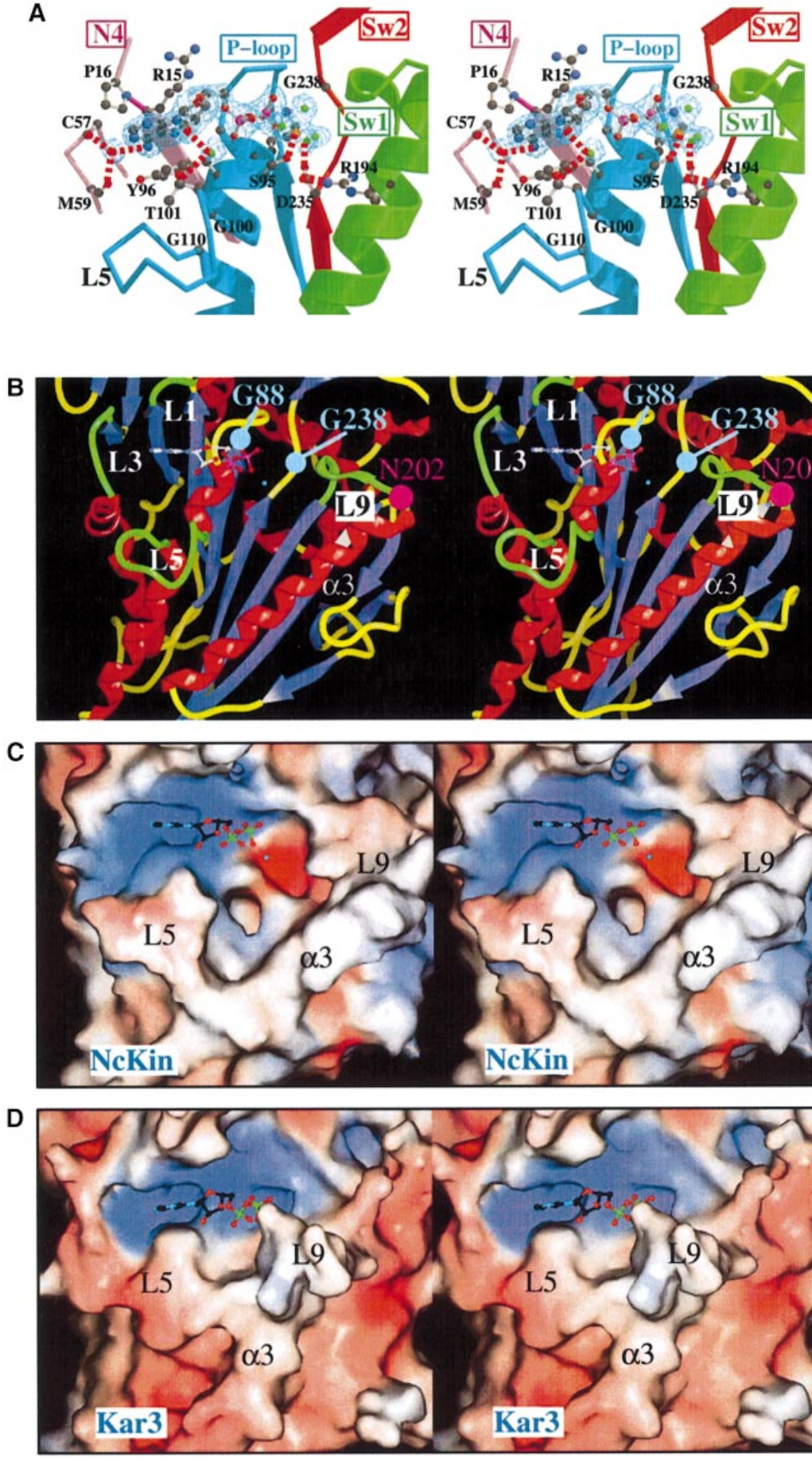
A
N4
P-loop
Sw2
Sw1
P16
R15
G238
C57
S95
R194
Y96
D235
M59
T101
G100
G110
L5
B
G88
L1
L3
N202
L9
α3
C
NcKin
D
Kar3

residues glycine and asparagine compared with NcKin, the bulge loop in the reverse motors tightens the entrance of the active site even further.

Salt bridges involved in nucleotide binding and switching

The structures of myosins in different nucleotide states, including ADP, ATP, AMP-PNP and ADP-VO_4, revealed that the movement of Sw1 and Sw2 was accompanied by the reversible formation of critical salt bridges. Thus, the salt bridge R238–E459 is formed in myosin only in a closed-cleft structure complexed with ADP-VO_4 (Smith and Rayment, 1996). We refer to the corresponding salt bridge as the inter-switch salt bridge type-A (SbA). Another important interaction is the hydrogen bond between the γ-phosphate and the amide of G457 observed in myosin II. To gain some insight into the ATPase mechanism of kinesin, we compared salt bridges and hydrogen bonds around the active site of NcKin with those of known kinesin structures (Figure 6). In all structures, at least one salt bridge was found, mostly between Sw1 and Sw2 (Table III). A unique feature of NcKin is that there are three inter-switch salt bridges (Figure 6). (i) The salt bridge E240–R207 is of the same type as that in RnKin and myosin complexed with ADP-VO_4 (SbA). (ii) The salt bridge between K257 (Sw2) and E204 (Sw1) in NcKin is of a new type, termed SbC. It can only be observed in NcKin because L11 is ordered in NcKin. This interaction is probably important for the stabilization of L11. (iii) The third salt bridge is between D235 and R194, named SbB. These residues are preserved throughout the family of kinesin proteins. The residues of SbB are connected with the Mg^{2+} ion via a water-mediated hydrogen bond. This means that this salt bridge is likely to play a role in the dissociation of the Mg^{2+} ion from the active site. It was shown that the disruption of the Mg^{2+} coordination is the key step for dissociation of the nucleotide GDP in $P21^{ras}$ GTPase, where the GEF-mediated displacement of the Sw1 region of ~15 Å is involved (Figure 5D) (Mittal *et al*., 1996; Boriack-Sjodin *et al*., 1998). Such a movement of Sw1 can be observed in NcKin in comparison with Sw1 of the other kinesins (Figure 5A and B). In the case of HsKin (Kull *et al*., 1996), only one intra-Sw1 salt bridge (E199–R203) can be found, here termed 'type-D' (SbD). The residues for the three types of salt bridge are preserved in all kinesins; however, the sets of salt bridges actually found in each structure are different (Figure 6B).

Interaction between the motor domain of NcKin and microtubules

We investigated the NcKin355-decorated MTs by cryo-electron microscopy of unstained vitrified samples and calculated the three-dimensional image reconstructions of the complexes. Since high resolution structures are available both for tubulin (Nogales *et al*., 1999) and NcKin (this work), one can fit the molecules into the electron density derived from cryo-electron microscopy (Figure 7A). The MT is shown with its plus end (= fast growing end) towards the top of the page so that the orientation of the attached kinesin is upside down, compared with Figure 1 (for details on the identification see Song and Mandelkow, 1993; Hoenger *et al*., 1998). The bulk of the interaction involves the C-terminal part of β-tubulin (helices H11 and H12) and the region α4–L12–α5 of NcKin. The interaction appears to be mediated mainly by electrostatic force. There are several negatively charged residues in helix H12 of β-tubulin (E420, D427 and E431 numbered according to the bovine β-tubulin sequence) which can accomplish electrostatic interactions with the positively charged residues in L12 and α5 of kinesin (K276 and R283). Indeed, the equivalent residue of R283 has been reported to have a pronounced influence on the binding and activity of HsKin (Woehlke *et al*., 1997), and positively charged insertions into L12 of kinesin ('K-loop') increase the interactions with MTs so that even monomeric kinesins (Kif1A) can become processive (Kikkawa *et al*., 2000). The β5–L8 region (red, Figure 7A and B) interacts with β-tubulin, as noted earlier (Sack *et al*., 1999). Of special interest is the position of L11, which is visible in the NcKin structure. Its main interaction appears not to be primarily with the central β-tubulin subunit (Figure 7B, green) but with the next α-tubulin subunit below (blue, towards the MT minus end) at the loop between helices H11 and H12. In addition, it is possible that L11 of kinesin interacts with the C-terminal region of β-tubulin in the adjacent protofilament (see Supplementary data available at *The EMBO Journal* Online). Since L11 of kinesin is in the vicinity of the γ-phosphate-sensing region, its interaction with α-tubulin probably plays a role during ATP hydrolysis. This might be one of the key elements in the MT-activated kinesin ATPase, consistent with the effect of mutant G243S (Figure 3). A third region of interest is the linker/neck region of kinesin. Although it is structurally not well defined, it emerges near the upper end of β-tubulin, on the right side of the protofilament (upper right corner in Figure 7A and B), and could thus interact with the C-terminal region of the next α-tubulin in the plus direction. This would explain why the opposite charges in kinesin's neck and tubulin's C-terminus are important for processive movement (Thorn *et al*., 2000; Wang and Sheetz, 2000).

Table II. Alignments of β-hairpin loop L5

NcKin	G^{100}	TSIDD**P**DGR	G^{110}
RnKin	G^{98}	KLHD**P**QLM	G^{107}
HsKin	G^{97}	KLHD**P**EGM	G^{106}
Ncd	G^{446}	V**P**ESV	G^{452}
Kar3	N^{486}	**P**GD	G^{490}

Discussion

Relationship of the Nckin structure to other kinesin motor domains

The main function of NcKin is in cell morphogenesis, especially in the longitudinal growth of the hyphae and the formation of a 'Spitzenkörper' (Seiler *et al*., 1997). NcKin is the fastest kinesin known so far (velocity ~2.6 μm/s *in vitro*; Kirchner *et al*., 1999). As shown here, the overall structure of the NcKin motor domain shows marked similarity to known kinesins (Figure 1). Most of them show ADP bound to the nucleotide-binding pocket, with two exceptions: (i) the RnKin motor domain was crystallized after hydrolysing ADP to AMP with apyrase,

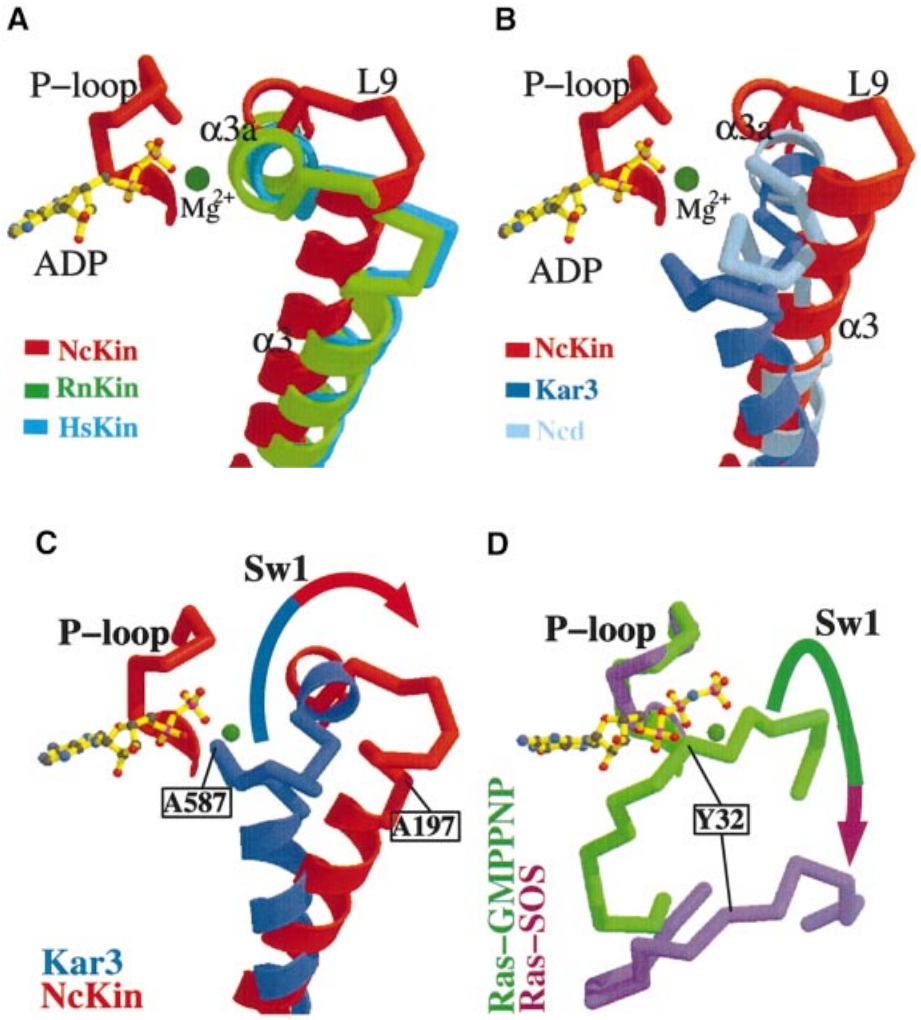

Fig. 5. Comparisons of the Sw1 structure of different proteins of the kinesin family. (**A**) Superposition of the Sw1 structures of NcKin (red) versus RnKin (green) and HsKin (cyan). (**B**) Superposition of NcKin (red) versus Ncd (light blue) and Kar3 (blue). The orientation of this model is rotated 90° around the *y*-axis and 30° around the *x*-axis compared with the view in Figure 1A and B. Displacement of Sw1 as an essential step for nucleotide exchange. (**C**) Superposition of Kar3 and NcKin (only the P-loop and Sw1 are shown). The displacement of Sw1 (A197 in NcKin and A587 in Kar3) between the two structures is ~15 Å. (**D**) Superposition of Ras-GTP and of the Ras–Sos structure. The displacement of Sw1 is also ~15 Å, measured by the distance at residue Y32 (Boriack-Sjodin *et al*., 1998).

without major changes in the nucleotide-binding pocket (Muller *et al*., 1999); and (ii) the monomeric kinesin Kif1a was crystallized with ADP and with AMP-PCP, an ATP analogue. The structures were broadly similar, but several local differences in mobile subdomains and loops were observed (Kikkawa *et al*., 2001). Some of them reflect differences between the members of the kinesin superfamily; others may be interpreted as representing different intermediate states available to all kinesins.

Broadly speaking, there are three variable regions among kinesins: (i) neck-linker and helix (β9–β10–α7); (ii) Sw2 region (L11–α4–L12–α5); and (iii) Sw1 region (α3–L9–α3a). The variable conformations found in different kinesins have been classified as ATP-like or ADP-like (Vale and Milligan, 2000). One distinction, found in G-proteins and myosin, is the 'closed' or 'open' nucleotide-binding pocket. Another criterion is the 'ordered' or 'disordered' neck helix α7, and neck-linker (strand β9–β10) 'attached' to or 'detached' from the core motor domain. Judging by the distance between the two conserved glycines in the P-loop and in Sw2, the nucleotide-binding pockets of kinesins are 'closed', reminiscent of ATP states in spite of bound ADP (Sack *et al*., 1999). The apparent discrepancy could be circumvented by considering more adequate measures of the nucleotide-binding pocket. Its size depends on the structure of L9 and thus Sw1 (Figure 4B, C and D and Supplementary data). The entrance of the nucleotide-binding pocket in NcKin is wider than in other structures because L9 is bent outwards from the pocket. Therefore, in NcKin, the rate-limiting step of the ATPase cycle, nucleotide exchange, should be faster than in other kinesins. The second criterion is based on the observation that in most kinesin structures the neck-linker and neck region is disordered. This led to a model of movement whereby the neck-linker is flexible in most states, allowing diffusional motion of the tethered head. However, when the trailing head, still attached to the MT, has ATP bound to the active site, the neck-linker docks to the core domain and prompts the tethered head to move towards the plus

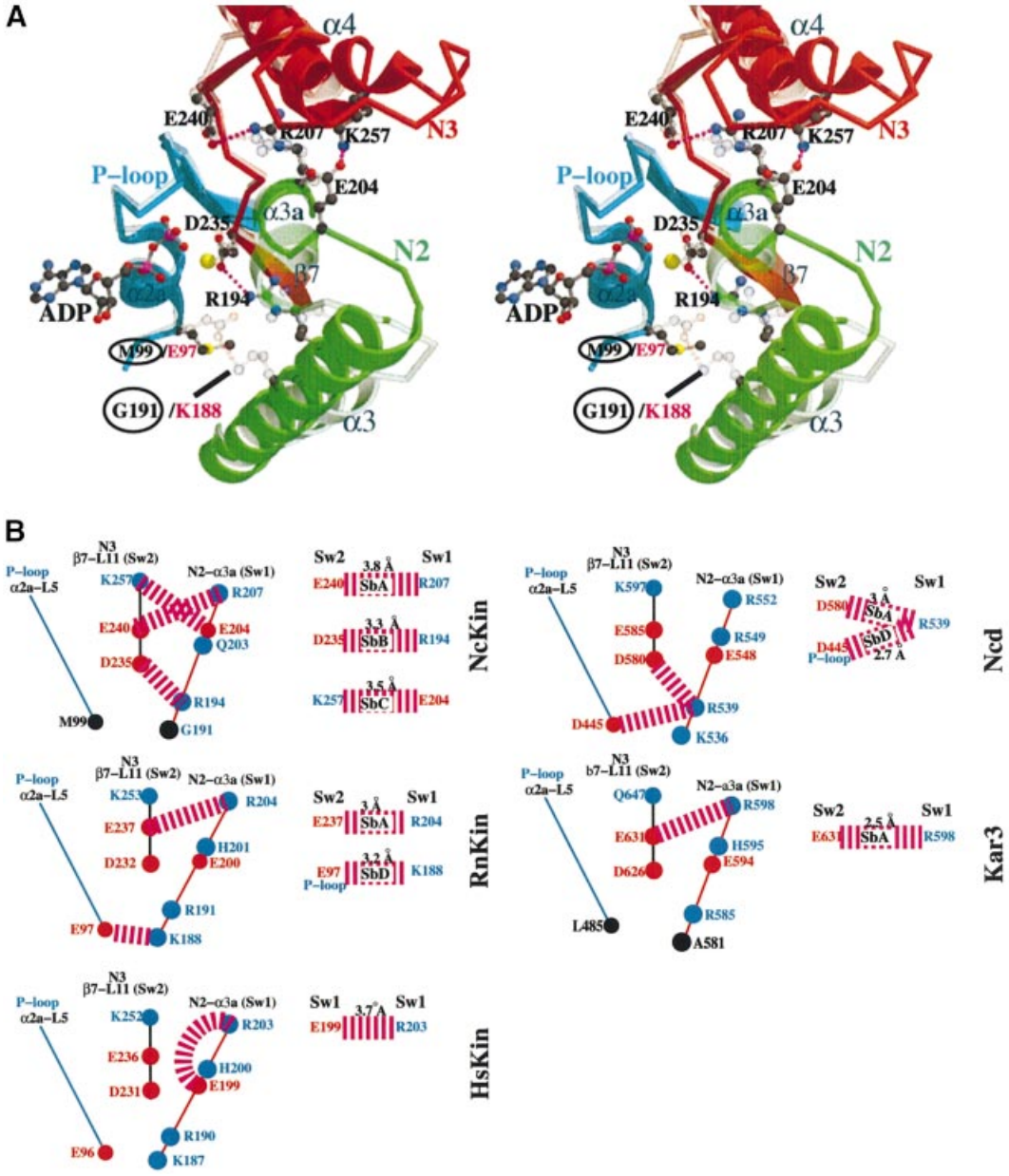

Fig. 6. Comparisons of salt bridges at the γ-phosphate-sensing region. (**A**) Stereo view of the superposition of NcKin (dark colour) and RnKin (pale colour). In NcKin, there are three inter-switch salt bridges and in RnKin there is only one. The salt bridge E97–K188 of RnKin cannot be formed in NcKin because at the corresponding positions there are no charged residues, which are Met99 and Gly191, respectively. (**B**) Summary of all known salt bridges of known kinesin structures.

end (Rice *et al*., 1999). According to this model, it has been proposed that the RnKin structure (Sack *et al*., 1997) should represent an ATP-like conformation, whereas the HsKin structure (Kull *et al*., 1996) is an ADP-like one (Vale and Milligan, 2000). The mitotic spindle kinesin Eg5, crystallized in the presence of ADP, has the neck-linker ordered but in an unusual orientation, roughly perpendicular to helix α6 (Turner *et al*., 2001). It was proposed that Eg5 may undergo transitions between two ordered states, whereas conventional kinesins cycle between ordered and disordered states of the neck-linker. Thus, Eg5 fits into the classification into ADP-like and ATP-like structures of the neck-linker, provided that the unusual, but ordered conformation of the neck-linker in Eg5 is analogous to the disordered state in conventional kinesin. On the other hand, the monomeric, plus-end motor Kif1a has the neck-linker disordered (invisible) both with ADP and with AMP-PCP (an ATP analogue) bound to the nucleotide-binding pocket (Kikkawa *et al*., 2001). In this case, one can argue that the neck-linker was engineered to include part of the linker of conventional kinesin, thus it may not be representative of the neck-linker's natural structure.

L11 has been rather elusive, as it is disordered under most conditions, yet it probably has an important function in coordinating local conformational changes. This can be assumed because of its central position between mobile regions (Sw1 and Sw2 regions) and since it directly

Table III. Salt bridges

	NcKin	RnKin	Ncd	Myosin (Dictyo)
SbA	E240(Sw2)–R207(Sw1)	E237(Sw2)–R204(Sw1)	D580(Sw2)–R539(Sw1)	E459(Sw2)–R238(Sw1)
SbB	D235(Sw2)–R194(Sw1)			D454(Sw2)–K241(Sw1)
SbC	K257(Sw2)–E204(Sw1)			
SbD		E97(P-loop)–K188(Sw1)	D445(P-loop)–R539	

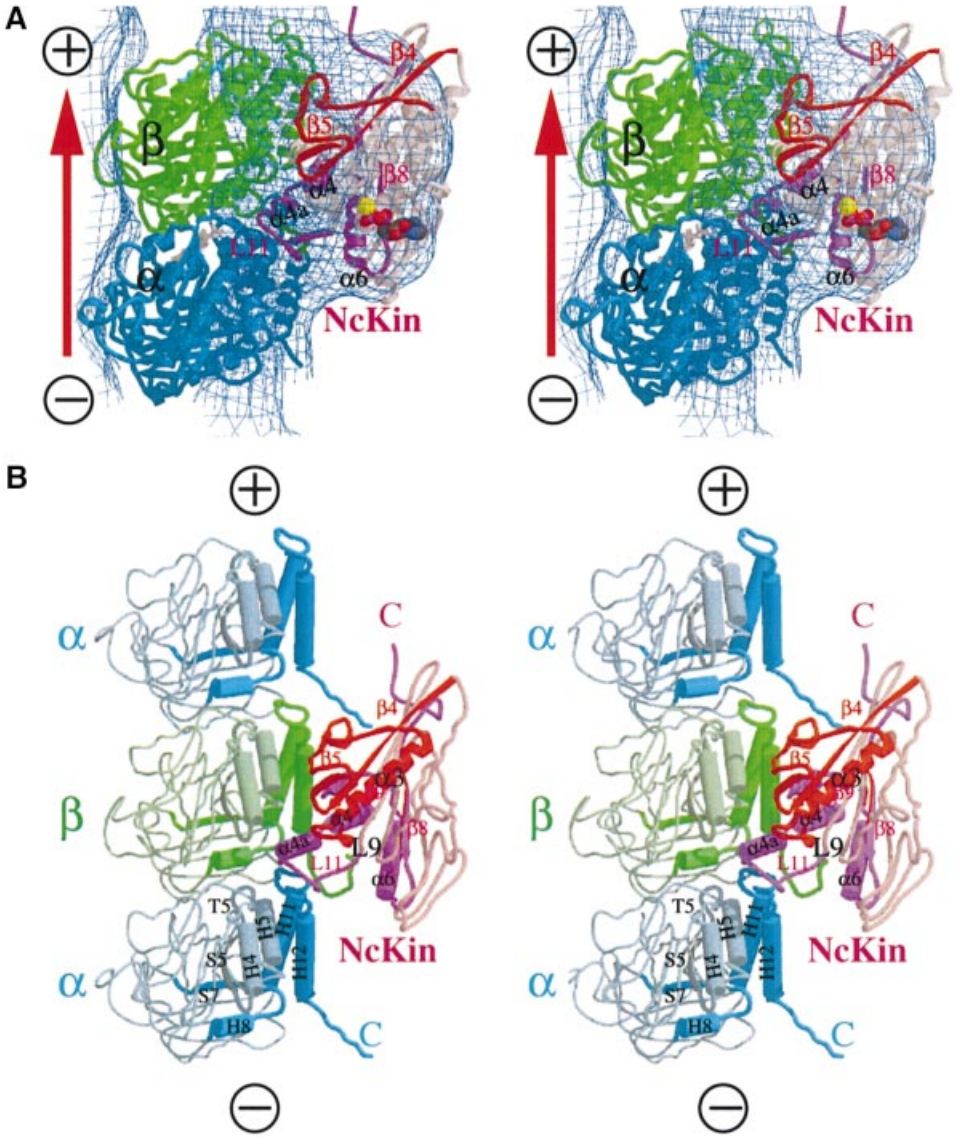

Fig. 7. Image reconstructions of MTs decorated with NcKin and interactions between them. Stereo views. (**A**) View from the side of a protofilament. Protein structures docked into the electron density are shown in green (β-tubulin), blue (α-tubulin) and grey/red (kinesin). The bound ADP is visible on the lower tip of kinesin. The bulk of the electron density of kinesin lies over a β-tubulin subunit, but there is some overlap with other subunits, especially the two flanking α-tubulin subunits within the same protofilament. (**B**) View from the side of a tubulin protofilament (i.e. tangential to the MT surface). Selected elements in the interacting regions are highlighted, α-helices as tubes, β-strands as ribbons. In NcKin, the elements L11, helix α4 (Sw2 region) and the region up to the C-terminus are purple, β4 and the β5/loop8 region (Sw1) are red. The tubulin subunits are blue (α-tubulin) and green (β-tubulin). The tubes show the near C-terminal helices H11 and H12, as well as helices H4, H5, H8 and adjacent loops. The C-terminal tail of tubulin (not visible in the structure due to disorder) has been drawn in arbitrary conformations in order to highlight potential interactions with kinesin (see text).

follows the LAGSE motif in Sw2. Indeed, mutations in this region strongly reduce the speed and ATPase activity, such as G243S in NcKin, S246F in *Drosophila* kinesin, and V238W in HsKin (Brendza *et al*., 1999; Xing *et al*., 2000). L11 may be required for flexible binding of the kinesin head to the MT, as suggested by Sosa *et al*. (2001)

who showed that MT-bound kinesin is still highly mobile in the ADP state, but immobile in the ATP, ADP·Pi or no-nucleotide states.

Superposition of various kinesin structures suggests that helices α4, α5 and the connecting loop L12 form a subdomain that is able to slide along the MT-facing surface of kinesin's core domain (Sack *et al*., 1999; Vale and Milligan, 2000). In HsKin, Kar3, Eg5 and Kif1a (all with ADP), this subdomain is in the 'up' position, while in RnKin (with ADP) and Kif1a (with AMPPCP) it is in the 'down' position (Kikkawa *et al*., 2001; Turner *et al*., 2001). Furthermore, helix α4 can rotate and change in length. In Eg5, helix α4 is 1.5 turns longer than in conventional kinesin (Turner *et al*., 2001). Consistent with this variability, α4 can assume different lengths in crystals of Kar3 (Yun *et al*., 2001). ATP at the active site seems to favour shortening of helix α4. In Kif1A, it is about two turns longer with ADP than with AMP-PCP (Kikkawa *et al*., 2001). Since the length of L11 is inversely related to the length of helix α4 (which comes next to L11), a correlation between the conformation of L11 and helix α4 would be expected. Thus, reversible melting and reformation of α4 could play an essential role in the mechanochemical cycle.

Structural implications for ATPase cycle and dynamic network of salt bridges

Transient-state kinetic studies of kinesin have helped to define the pathway of ATP turnover (Hackney, 1996; Ma and Taylor, 1997; Gilbert *et al*., 1998). The release of ADP from the active site determines the overall rate-limiting step in the catalytic cycle. This step will be accelerated by MTs so that the MT serves as a nucleotide exchange factor (AEF analogous to GEF of G-proteins). It has been shown that myosin can be found in the same conformation in spite of different bound ATP analogues (Holmes and Geeves, 2000). This implies that different conformations have similar energies and that the partner protein, F-actin or MT, can force controlled conformational transitions along the reaction pathway. It is currently difficult to understand how the presence of one phosphate can lead to conformational changes of the MT-binding site (the cluster α4, L12, α5 and L13). As discussed before, this is one of the regions of high diversity among the known kinesin structures. However, conformational alterations are likely to consist of a cascade of small events, mediated by the formation of specific salt bridges or hydrogen bonds (Furch *et al*., 1999). We therefore examined salt bridges near the γ-phosphate-sensing region formed by Sw1 and 2. Generally, two types of inter-switch salt bridges can be found, SbA and SbB. The residues responsible for those salt bridges are conserved throughout kinesins and myosins (Table III).

The SbA is found in NcKin, RnKin and in myosin only in the 'closed' conformation (PDB: 1BR1, 1BR4, 1VOM). The closed conformation in myosin is characterized by the amide of conserved Gly457 forming a hydrogen bond to the γ-phosphate analogue, postulated to be the transition state of the myosin-ATPase. Interestingly, the SbA is not formed in all the kinesin structures (Figure 6B). The SbB is formed again in NcKin and myosin but not in any other plus-directed kinesin motors, but it is present in Ncd. There is only one intra-switch salt bridge in HsKin. There is an additional salt bridge in RnKin between the P-loop (E97) and Sw1 (K188). A similar salt bridge is also present in Ncd (D580–R539; Figure 6B). This salt bridge has been postulated to form while the SbA is breaking when the enzyme makes the transition from the ATP state to the ADP state (Wriggers and Schulten, 1998). However, there are no charged residues at the corresponding positions in NcKin, which are replaced instead by M99 and G191. This is also the case for Kar3 (L485 and A581).

Comparisons of salt bridges in kinesins and myosins suggest the following: (i) there are conserved charged residues in the γ-phosphate-sensing region, Sw1 and Sw2; and (ii) different sets of salt bridges can be observed in different structures. The switches are intrinsically mobile and therefore it is possible that any of the salt bridges observed so far may form in every enzyme at a certain stage during the path of the ATPase. Even though we may be able to observe in a given structure a given set of salt bridges, this may be due to stabilization by particular circumstances, such as crystallization conditions. This conclusion is also evident if one considers that myosin can adopt both conformations of either an open or closed state in the presence of ADP-BeF_3 (Geeves and Holmes, 1999). From this observation, one can deduce that the motor proteins might be in a dynamic conformational state. The role of the track (MT or F-actin) is probably to pave the way out of this non-directed dynamic conformational path to proceed in an ordered direction, resulting in an ATP-driven motor activity. Such a conformational dynamic has already been suggested by Vale and Milligan (2000), when they compared the two structures RnKin and HsKin. Here we venture one step further. The first step is the breach of the bond of the bridge oxygen of β- and γ-phosphate, whereby the peptide flip of the conserved glycine occurs. Such peptide flips have been observed in myosin (PDB: 1VOM versus 1MMD). Some salt bridges in the path can be rearranged, and the potential salt bridges are noted in Figure 6B. After dissociation of γ-phosphate, the associated ADP has to be replaced by ATP, which is the point where the MT comes into play.

The Mg^{2+} cofactor plays an important role in nucleotide exchange and hydrolysis of small G-proteins (Mittal *et al*., 1996). Crystallographic studies of the Ha-Ras–Sos complex have revealed that the GEF dislocates the Sw1 region, thereby disrupting the Mg^{2+} coordination (Boriack-Sjodin *et al*., 1998). This results in the destabilization of GDP binding and accelerates GDP dissociation. Figure 5C and D shows a similar displacement of the Sw1 region if one compares Kar3 with NcKin. To a lesser extent, this is also the case when the structure of NcKin is superimposed with that of HsKin and RnKin. Given that ADP–ATP exchange is rate limiting in the overall reaction, where an MT comes into play as an AEF, this may explain why NcKin has a higher ATPase activity than other kinesins. In the case of the GEF, the displacement of Sw1 occurs via insertion of an α-helix from Sos. Whether the exact mechanism of AEF activity of the tubulin would be the same as for the G-protein will be a matter of further study.

Interaction between NcKin and microtubules

Kinesin moves along MTs, and therefore the function of kinesin can only be understood in terms of its interaction with MTs. The NcKin–MT complex can be studied by

cryo-electron microscopy and image reconstruction. Figure 7 shows that the orientation of the motor domain is very similar to that obtained previously with other types of kinesin (Hoenger *et al*., 1998, 2000), in good agreement with the results obtained by other authors (e.g. Sosa *et al*., 1997; Kikkawa *et al*., 2001). As diagrammed in Figure 7, the bulk of the motor domain packs against a central β-tubulin subunit, mainly involving the 'Sw2 cluster' α4–L12–α5, which lies across the outermost α-helix H12 of β-tubulin, and the region β5a/b–L8, which leans against the upper end and side of α-helix H12 in β-tubulin. This agrees well with results showing that major cross-links occur between kinesin and β-tubulin (Song and Mandelkow, 1993), and with mutagenesis studies showing that residues in the α4–L12–α5 region strongly affect kinesin's interactions with MTs (Woehlke *et al*., 1997).

Of special interest in our case is the position of elements not visible previously, such as L11, or with a different conformation, such as the C-terminal neck region. L11 protrudes into a cleft between the central β-tubulin and the lower α-tubulin (in the minus direction, Figure 7B) before it links up, via α4a, to the Sw2 helix α4. It might therefore function as an anchor for the amplification of any movement occurring on Sw2 during the ATPase cycle (such as rotation or tilting; Vale and Milligan, 2000; Kikkawa *et al*., 2001; Yun *et al*., 2001). Note that kinesin's L11 fits snugly against the loop connecting the two outermost helices H11 and H12 in α-tubulin. This therefore represents one of the inter-subunit interactions along a protofilament, on the lower end of the kinesin subunit in Figure 7. Another one occurs at the upper end, towards the plus-end of the protofilament, where the neck region of kinesin approaches the C-terminus of α-tubulin. These two regions are highly mobile: in tubulin, the C-terminus is not visible due to disorder (Nogales *et al*., 1999), and was therefore inserted here arbitrarily in an extended conformation in order to underscore the space it could sweep out. The neck region of NcKin has the same general orientation as in the well-ordered RnKin structure, tangentially to the MT wall (Figure 7A). It is likely that they interact because of their complementary charges (glutamine residues on tubulin, lysine residues in the kinesin neck). Indeed, cross-linking studies support such an interaction (Tucker and Goldstein, 1997), as well as mutagenesis experiments on the neck region which show that the charges are important for kinesin's processive movement (Thorn *et al*., 2000; Wang and Sheetz, 2000).

Materials and methods

Protein expression, purification and crystallization

Kinesin was expressed in the *Escherichia coli* strain BL21(DE3)-CodonPlusRIL (Stratagene) in LB medium with 50 μg/ml carbenicillin. Cells were grown at 37°C until 0.6 OD_{600}, expression was induced by adding 1 mM isopropyl-β-D-thiogalactopyranoside (IPTG) and cells were grown for another 16 h at 25°C. Cells were harvested and resuspended in lysis buffer [20 mM PIPES pH 6.91, 1 mM each EGTA, dithiothreitol (DTT), $MgCl_2$ and 50 mM NaCl], and the crude extract was obtained by a double passage through a French press (Aminco) and high speed centrifugation. The pure protein NcKin355 was obtained after ion exchange column chromatography steps (phosphocellulose and MonoQ) followed by gel filtration (Sephadex 200) in a buffer containing 20 mM Tris pH 7.9, 5 mM $MgCl_2$ and 0.5 mM ADP. The protein was concentrated up to 20 mg/ml and stored at –20°C. It was crystallized by the vapour diffusion method in a sitting drop against 17.5% PEGMME 2000 (Fluka), 100 mM HEPES pH 6.5–7.5 and 3% glycerol. The protein concentrations were 7.5–15 mg/ml. Small crystals formed within a week and grew to their maximal size (50 × 50 × 500 μm) during a period of 4–5 weeks at 19°C. For data collection at –180°C, the reservoir solution was replaced by cryo buffer (100 mM HEPES pH 6.5–7.5, 17.5% PEGMME 2000, 15% glycerol).

X-ray data collection and structure determination

Using the beamline BW6 at DESY equipped with a CCD detector (MarResearch), a complete data set was obtained to 2.3 Å resolution. The crystals had an orthorhombic lattice and space group $P2_12_12_1$ (a = 51.98 Å, b = 72.73 Å, c = 84.93 Å) with one molecule in the asymmetric unit. The data were reduced using the program package XDS (Kabsch, 1993). The phase information was calculated using molecular replacement methods in the program package CNS (Brünger *et al*., 1998). The Matthews parameter was Vm = 2.07 $Å^3$/D, corresponding to 40.6% solvent content. The search model consisted of the RnKin monomer structure (PDB: 2KIN; Sack *et al*., 1997), excluding L11, residues 239–251 and the C-terminal linker and neck region (residues 330–354). A clear solution with a correlation factor of 42.4% was found. The model was built using the program O (Jones *et al*., 1991). Residues 7–329 comprising the core motor domain of NcKin could be fitted into the initial map. During the refinement, the chain could be extended up to 355 amino acids, including the N-terminal residues and the C-terminal linker/neck region. Prior to refinement, 5.6% of the data were selected randomly as a set of test reflections. Simulated annealing torsion angle refinement against amplitude maximum likelihood targets was performed in CNS version 1.0 (Brünger *et al*., 1998). Energy minimization and individual B-factor refinement were also used in the same program. Every cycle was followed by rebuilding the structure in program O. Several cycles of simulated annealing were performed until no significant positive peaks remained detectable in the $F_o - F_c$ map. After 20 cycles, the crystallographic R-factor fell from 48.4 to 21% and the R_{free} from 48 to 25.6%. Apart from the 355 residues, the current model contains MgADP and 128 water molecules; however, the electon density for residues 332–355 was weak. Stereochemical correctness of the model was verified by the program PROCHECK (Laskowski *et al*., 1996). Figures were prepared using MOLSCRIPT (Kraulis, 1991) and SPOCK (Christopher, 1998) and rendered using the program Raster3D (Merrit, 1994).

Cryo-electron microscopy and image reconstruction of MTs decorated with NcKin

The experimental procedures were essentially as described (Hoenger *et al*., 1998). Briefly, MTs from pig brain tubulin were polymerized for 20 min at 37°C in 80 mM PIPES pH 6.8, 2 mM $MgCl_2$, at a concentration of 2.5 mg/ml and in the presence of 5% (v/v) dimethylsulfoxide (DMSO), 2 mM GTP and 20 μM taxol. Decoration of polymerized MTs with NcKin motor domains was performed in solution at a final tubulin concentration of ~10 μM and a final kinesin concentration of ~15–20 μM in the presence of 2 mM AMP-PNP or after incubation with apyrase to remove ADP. Samples were incubated for 2 min, adsorbed to holey carbon grids for 1 min and quick-frozen in liquid ethane. Cryo-electron microscopy was performed on a Philips CM120-BioTWIN microscope, using a GATAN-626 cryo-holder. Images were recorded on Kodak SO-163 electron microscopy film at a defocus around –1.5 to 2.0 μm. For image reconstruction, micrographs were digitized using a Zeiss-SCAI scanner. Suitable 15-protofilament/2-start MTs were helically reconstructed by using the program suite PHOELIX.

Protein Data Bank accession code

The coordinates have been deposited in the Protein Data Bank (access code 1GOJ).

Supplementary data

Supplementary data for this paper are available at *The EMBO Journal* Online.

Acknowledgements

We are grateful to H.D.Bartunik and the staff for access to the Max-Planck beamline BW6 at DESY, Hamburg. We thank A.Kallipolitou, M.Schleicher and F.Schwarz (Munich) for active help in the initial stages of this work, S.Hoffmann and H.Deisemann (Hamburg) for excellent technical assistance, and E.-M.Mandelkow (Hamburg) for numerous

discussions throughout this work. The project was supported by the Deutsche Forschungsgemeinschaft, VW-Stiftung and Fonds der Chemischen Industrie.

References

Boriack-Sjodin,P.A., Margarit,S.M., Bar-Sagi,D. and Kuriyan,J. (1998) The structural basis of the activation of Ras by Sos. *Nature*, **394**, 337–343.

Brendza,K.M., Rose,D.J., Gilbert,S.P. and Saxton,W.M. (1999) Lethal kinesin mutations reveal amino acids important for ATPase activation and structural coupling. *J. Biol. Chem.*, **274**, 31506–31514.

Brünger,A.T. *et al*. (1998) Crystallography and NMR system: a new software suite for macromolecular structure determination. *Acta Crystallogr. D*, **54**, 905–921.

Christopher,J.A. (1998) *SPOCK: The Structural Properties Observation and Calculation Kit* (Program Manual). The Center for Macromolecular Design, Texas A&M University, College Station, TX.

Coleman,D.E. and Sprang,S.R. (1999) Reaction dynamics of G-protein catalyzed hydrolysis of GTP as viewed by X-ray crystallographic snapshots of Giα1. *Methods Enzymol.*, **308**, 70–92.

Crevel,I., Carter,N., Schliwa,M. and Cross,R. (1999) Coupled chemical and mechanical reaction steps in a processive *Neurospora* kinesin. *EMBO J.*, **18**, 5863–5872.

Endow,S.A. and Komma,D.J. (1997) Spindle dynamics during meiosis in *Drosophila* oocytes. *J. Cell Biol.*, **137**, 1321–1336.

Furch,M., Fujita-Becker,S., Geeves,M.A., Holmes,K.C. and Manstein, D.J. (1999) Role of the salt-bridge between switch-1 and switch-2 of *Dictyostelium* myosin. *J. Mol. Biol.*, **290**, 797–809.

Geeves,M.A. and Holmes,K.C. (1999) Structural mechanism of muscle contraction. *Annu. Rev. Biochem.*, **68**, 687–728.

Gilbert,S.P., Moyer,M.L. and Johnson,K.A. (1998) Alternating site mechanism of the kinesin ATPase. *Biochemistry*, **37**, 792–799.

Goldstein,L.S. and Philp,A.V. (1999) The road less traveled: emerging principles of kinesin motor utilization. *Annu. Rev. Cell Dev. Biol.*, **15**, 141–183.

Gulick,A.M., Song,H., Endow,S.A. and Rayment,I. (1998) X-ray crystal structure of the yeast Kar3 motor domain complexed with Mg·ADP to 2.3 Å resolution. *Biochemistry*, **37**, 1769–1776.

Gulick,A.M., Bauer,C.B., Thoden,J.B., Pate,E., Yount,R. and Rayment,I. (2000) X-ray structures of *Dictyostelium discoideum* myosin motor domain with six nucleotide analogues. *J. Biol. Chem.*, **275**, 398–408.

Hackney,D.D. (1996) The kinetic cycles of myosin, kinesin and dynein. *Annu. Rev. Physiol.*, **58**, 731–750.

Hilgenfeld,R. (1995) How do the GTPases really work? *Nature Struct. Biol.*, **2**, 3–6.

Hoenger,A., Sack,S., Thormahlen,M., Marx,A., Muller,J., Gross,H. and Mandelkow,E. (1998) Image reconstructions of microtubules decorated with monomeric and dimeric kinesins: comparison with X-ray structure and implications for motility. *J. Cell Biol.*, **141**, 419–430.

Hoenger,A., Thormahlen,M., Diaz-Avalos,R., Doerhoefer,M., Goldie, K.N., Muller,J. and Mandelkow,E. (2000) A new look at the microtubule binding patterns of dimeric kinesins. *J. Mol. Biol.*, **297**, 1087–1103.

Holmes,K.C. and Geeves,M.A. (2000) The structural basis of muscle contraction. *Philos. Trans. R. Soc. Lond. Ser. B Biol. Sci.*, **355**, 419–431.

Houdusse,A., Szent-Gyorgyi,A.G. and Cohen,C. (2000) Three conformational states of scallop myosin S1. *Proc. Natl Acad. Sci. USA*, **97**, 11238–11243.

Jones,T.A., Zou,J.Y., Cowan,S.W. and Kjeldgaard,M. (1991) Improved methods for building protein models in electron density maps and the location of errors in these models. *Acta Crystallogr.*, **A47**, 110–119.

Kabsch,W.J. (1993) Automatic processing of rotation diffraction data from crystals of initially unknown symmetry and cell constants. *Appl. Crystallogr.*, **26**, 795–800.

Kikkawa,M., Okada,Y. and Hirokawa,N. (2000) 15 Å resolution model of the monomeric kinesin motor, KIF1A. *Cell*, **100**, 241–252.

Kikkawa,M., Sablin,E.P., Okada,Y., Yajima,H., Fletterick,R.J. and Hirokawa,N. (2001) Switch-based mechanism of kinesin motors. *Nature*, **411**, 439–445.

Kirchner,J., Seiler,S., Fuchs,S. and Schliwa,M. (1999) Functional anatomy of the kinesin molecule *in vivo*. *EMBO J.*, **18**, 4404–4413.

Kozielski,F., Sack,S., Marx,A., Thormahlen,M., Schonbrunn,E., Biou,V., Thompson,A., Mandelkow,E.M. and Mandelkow,E. (1997) The crystal structure of dimeric kinesin and implications for microtubule-dependent motility. *Cell*, **91**, 985–994.

Kraulis,P.J. (1991) MOLSCRIPT: a program to produce both detailed and schematic plots of protein structures. *J. Appl. Crystallogr.*, **24**, 946–950.

Kull,F.J., Sablin,E.P., Lau,R., Fletterick,R.J. and Vale,R.D. (1996) Crystal structure of the kinesin motor domain reveals a structural similarity to myosin. *Nature*, **380**, 550–555.

Kull,F.J., Vale,R.D. and Fletterick,R.J. (1998) The case for a common ancestor: kinesin and myosin motor proteins and G proteins. *J. Muscle Res. Cell Motil.*, **19**, 877–886.

Laskowski,R.A., Rullmannn,J.A., MacArthur,M.W., Kaptein,R. and Thornton,J.M. (1996) AQUA and PROCHECK-NMR: programs for checking the quality of protein structures solved by NMR. *J. Biomol. NMR*, **8**, 477–486.

Ma,Y.Z. and Taylor,E.W. (1997) Interacting head mechanism of microtubule–kinesin ATPase. *J. Biol. Chem.*, **272**, 724–730.

Merrit,E.A., Murphy,M.E.P. (1994) Raster3D version 2.0. A program for photorealistic molecular graphics. *Acta Crystallogr. D*, **50**, 869–873.

Mittal,R., Ahmadian,M.R., Goody,R.S. and Wittinghofer,A. (1996) Formation of a transition-state analog of the Ras GTPase reaction by Ras-GDP, tetrafluoroaluminate and GTPase-activating proteins. *Science*, **273**, 115–117.

Muller,J., Marx,A., Sack,S., Song,Y.H. and Mandelkow,E. (1999) The structure of the nucleotide-binding site of kinesin. *Biol. Chem.*, **380**, 981–992.

Nogales,E., Whittaker,M., Milligan,R.A. and Downing,K.H. (1999) High-resolution model of the microtubule. *Cell*, **96**, 79–88.

Rayment,I. (1996) Kinesin and myosin: molecular motors with similar engines. *Structure*, **4**, 501–504.

Rice,S. *et al*. (1999) A structural change in the kinesin motor protein that drives motility. *Nature*, **402**, 778–784.

Sablin,E.P., Kull,F.J., Cooke,R., Vale,R.D. and Fletterick,R.J. (1996) Crystal structure of the motor domain of the kinesin-related motor ncd. *Nature*, **380**, 555–559.

Sablin,E.P., Case,R.B., Dai,S.C., Hart,C.L., Ruby,A., Vale,R.D. and Fletterick,R.J. (1998) Direction determination in the minus-end-directed kinesin motor ncd. *Nature*, **395**, 813–816.

Sack,S., Muller,J., Marx,A., Thormahlen,M., Mandelkow,E.M., Brady, S.T. and Mandelkow,E. (1997) X-ray structure of motor and neck domains from rat brain kinesin. *Biochemistry*, **36**, 16155–16165.

Sack,S., Kull,F.J. and Mandelkow,E. (1999) Motor proteins of the kinesin family. Structures, variations and nucleotide binding sites. *Eur. J. Biochem.*, **262**, 1–11.

Sawin,K.E., Mitchison,T.J. and Wordeman,L.G. (1992) Evidence for kinesin-related proteins in the mitotic apparatus using peptide antibodies. *J. Cell Sci.*, **101**, 303–313.

Scheffzek,K., Ahmadian,M.R., Wiesmuller,L., Kabsch,W., Stege,P., Schmitz,F. and Wittinghofer,A. (1998) Structural analysis of the GAP-related domain from neurofibromin and its implications. *EMBO J.*, **17**, 4313–4327.

Scheidig,A.J., Franken,S.M., Corrie,J.E., Reid,G.P., Wittinghofer,A., Pai,E.F. and Goody,R.S. (1995) X-ray crystal structure analysis of the catalytic domain of the oncogene product p21H-ras complexed with caged GTP and mant dGppNHp. *J. Mol. Biol.*, **253**, 132–150.

Seiler,S., Nargang,F.E., Steinberg,G. and Schliwa,M. (1997) Kinesin is essential for cell morphogenesis and polarized secretion in *Neurospora crassa*. *EMBO J.*, **16**, 3025–3034.

Smith,C.A. and Rayment,I. (1996) X-ray structure of the magnesium(II)·ADP·vanadate complex of the *Dictyostelium discoideum* myosin motor domain to 1.9 Å resolution. *Biochemistry*, **35**, 5404–5417.

Song,Y.H. and Mandelkow,E. (1993) Recombinant kinesin motor domain binds to β-tubulin and decorates microtubules with a B surface lattice. *Proc. Natl Acad. Sci. USA*, **90**, 1671–1675.

Sosa,H., Hoenger,A. and Milligan,R.A. (1997) Three different approaches for calculating the three-dimensional structure of microtubules decorated with kinesin motor domains. *J. Struct. Biol.*, **118**, 149–158.

Sosa,H., Peterman,E.J., Moerner,W.E. and Goldstein,L.S. (2001) ADP-induced rocking of the kinesin motor domain revealed by single-molecule fluorescence polarization microscopy. *Nature Struct. Biol.*, **8**, 540–544.

Steinberg,G. and Schliwa,M. (1996) Characterization of the biophysical and motility properties of kinesin from the fungus *Neurospora crassa*. *J. Biol. Chem.*, **271**, 7516–7521.

Thormahlen,M., Marx,A., Sack,S. and Mandelkow,E. (1998) The coiled-coil helix in the neck of kinesin. *J. Struct. Biol.*, **122**, 30–41.

Thorn,K.S., Ubersax,J.A. and Vale,R.D. (2000) Engineering the processive run length of the kinesin motor. *J. Cell Biol.*, **151**, 1093–1100.

Tucker,C. and Goldstein,L.S.B. (1997) Probing the kinesin–microtubule interaction. *J. Biol. Chem.*, **272**, 9481–9488.

Turner,J., Anderson,R., Guo,J., Beraud,C., Fletterick,R. and Sakowicz,R. (2001) Crystal structure of the mitotic spindle kinesin Eg5 reveals a novel conformation of the neck-linker. *J. Biol. Chem.*, **276**, 25496–25502.

Vale,R.D. and Milligan,R.A. (2000) The way things move: looking under the hood of molecular motor proteins. *Science*, **288**, 88–95.

Wang,Z. and Sheetz,M.P. (2000) The C-terminus of tubulin increases cytoplasmic dynein and kinesin processivity. *Biophys. J.*, **78**, 1955–1964.

Woehlke,G. and Schliwa,M. (2000) Walking on two heads: the many talents of kinesin. *Nature Rev. Mol. Cell. Biol.*, **1**, 50–58.

Woehlke,G., Ruby,A.K., Hart,C.L., Ly,B., Hom-Booher,N. and Vale, R.D. (1997) Microtubule interaction site of the kinesin motor. *Cell*, **90**, 207–216.

Wriggers,W. and Schulten,K. (1998) Nucleotide-dependent movements of the kinesin motor domain predicted by simulated annealing. *Biophys. J.*, **75**, 646–661.

Xing,J., Wriggers,W., Jefferson,G.M., Stein,R., Cheung,H.C. and Rosenfeld,S.S. (2000) Kinesin has three nucleotide-dependent conformations. Implications for strain-dependent release. *J. Biol. Chem.*, **275**, 35413–35423.

Yun,M., Zhang,X., Park,C.G., Park,H.W. and Endow,S.A. (2001) A structural pathway for activation of the kinesin motor ATPase. *EMBO J.*, **20**, 2611–2618.

Received August 2, 2001; revised September 14, 2001; accepted September 21, 2001